



TECHNICAL NOTE

A Novel Approach to Water Based Condensation Growth of Aerosols

Aaron Collins, William Dick, Francisco Romay

MSP Corporation, Shoreview, MN

04 January 2012

INTRODUCTION

A common working fluid used in the continuous flow condensation particle counter (CPC) is n-butanol. The general concept of most laminar, thermally diffusive CPC's using this working fluid is to first pass the aerosol through a warm, wet-walled saturator (Agarwal and Sem, 1980; Bricard et al 1976). The increased temperature and butanol-wetted walls result in a flux of vapor into the aerosol stream and in an increase in the bulk temperature of the aerosol flow. Once the aerosol is fully saturated with vapor, it is passed through a laminar-flow, chilled-wall condenser. Because of the large difference between the thermal diffusivity of air ($2.0E-5 \text{ m}^2/\text{sec}$) and the vapor diffusivity of butanol ($8.4E-6 \text{ m}^2/\text{sec}$) the thermal flux of the gas to the chilled wall occurs at a much greater rate than the butanol vapor flux to the wall. This results in regions of super-saturation occurring in a central core. Super-saturation, S , is defined as,

$$S = p_v / P_{sat}(T) \quad \text{Equation 1}$$

where, p_v is the partial pressure of the vapor, and P_{sat} is the temperature dependent saturation vapor pressure.

Figure 1 depicts a typical super-saturation profile for a butanol CPC, in which a vapor-laden aerosol at 35°C is introduced into a chilled-wall condenser operating at 5°C .

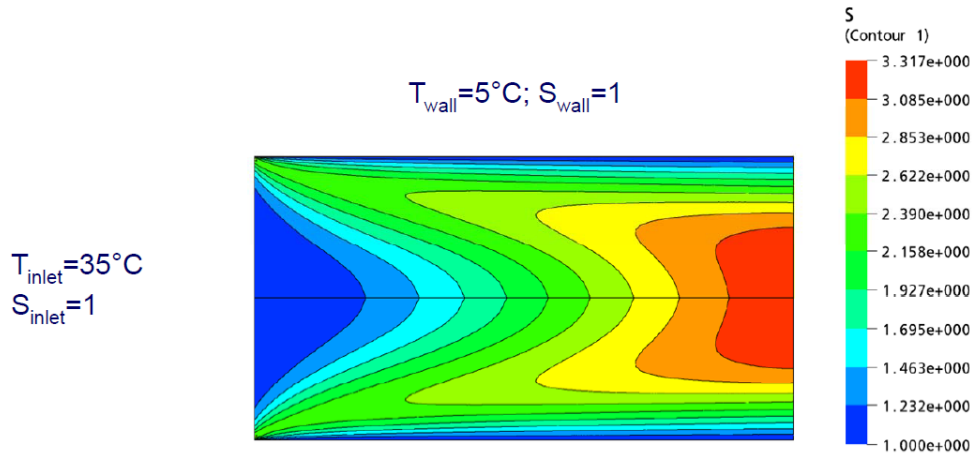


Figure 1 – Super-saturation profiles for a traditional butanol CPC

Water is a more attractive choice than butanol for a working fluid in some applications because it is environmentally benign. The approach described above, however, does not work if the working fluid is replaced with water. The vapor diffusivity for water vapor in air is $2.55E-5 \text{ m}^2/\text{s}$, roughly 1.3 times the thermal diffusivity of air. Flux of water vapor to the walls occurs at a faster rate than the thermal flux. Regions of super saturation form near the wall surface (Figure 2), where the incoming vapor flux from the core exceeds the thermal flux. This results in a large majority of the flow passing through regions of low super-saturation, yielding increased activation diameter and a reduced particle growth rate.

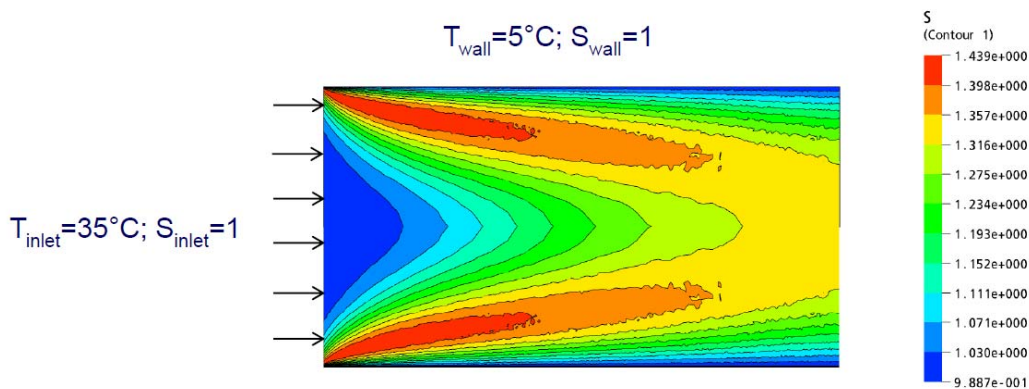


Figure 2 – Super-saturation profiles for a chilled-wall condenser with water vapor as the working fluid



CFD SIMULATION OF SINGLE-FLOW MIXING

To overcome the inability of the laminar flow condenser to work with water, a new method was developed which provides a uniform super-saturation profile with the traditional arrangement in which warm, vapor aerosol flows into a chilled growth section. This patent-pending (Liu et al, 2011) single-flow mixing (SFM) technique uses a small chilled-wall growth section. The flow is introduced into the base of the growth section via a large-diameter tangential inlet (Figure 3). The tangential inlet forces the incoming flow to travel along the perimeter of the lower portion of the growth section. This makes the internal flow field non-uniform and thus results in mixing between the incoming flow and the existing interior flow volume. This mixing action results in a relatively spatially homogenous super-saturation profile as the flow approaches the outlet.



Figure 3 – SFM Internal Geometry

To verify the internal flow field works as conceived, a computational fluid dynamics (CFD) flow simulation was performed to predict super-saturation profiles and Kelvin-equivalent activation diameters. The system was modeled using commercially available CFD software (Ansys CFX 10.0) to provide flow, temperature and vapor profiles within the SFM growth section. The fluid motion within the volume was modeled as laminar flow based on the low Reynolds number at the inlet, as well as in the internal volume. A diffusive transport model was used to simulate the mass transfer of water vapor from the incoming flow to the walls.



A temperature-dependent vapor diffusivity was used to provide an accurate model for the SFM technique. A second-order polynomial is fit to the temperature-dependent diffusion coefficient data provided by Bolz and Tuve (1976):

$$D(m^2 / s)_{air,water} = -2.775E - 6 + 4.479E8T + 1.656E - 10T^2 \quad \text{Equation 2}$$

where T is the absolute gas temperature in degrees Kelvin. Using the integrated mesh generator included within the CFD program, a tetrahedron mesh was generated with 296,233 nodes and approximately 1.5 million elements (Figure 4). The resulting mesh was refined during execution with a vapor concentration gradient and velocity gradient refinement scheme.

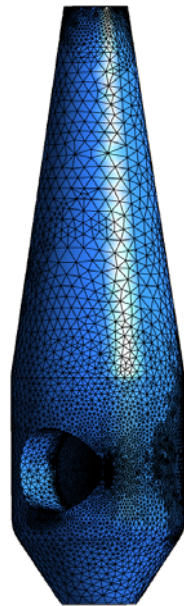


Figure 4- Mesh used for CFD Simulation

Boundary conditions for this simulation consist of an inlet flow rate of 1.00 L/min, an inlet temperature of 35°C, and an inlet water vapor concentration of 100% RH. The wall boundary conditions consist of a no-slip velocity condition, a fixed wall temperature of 5°C, and a wall vapor concentration of 100% RH. This water vapor boundary condition assumes that the wall is fully wetted.

The simulation was solved using the integrated solver, with convergence criteria set to 1E-6 for the root mean square (RMS) residuals. This solution value was achieved after approximately 600 outer loop iterations.

The expected level of non-uniformity in the flow is verified by the streamline plots shown in Figure 5. The importance of the tangential inlet is evident: the initial phase of mixing is induced by the tangential inlet flow striking the outer wall and being forced to begin a cyclonic turn. This rotation, counter-clockwise when viewed from the top



down, provides the effective mixing mechanism to reduce local areas of high super-saturation that would typically be generated in a linear laminar flow system (i.e., Figure 2).

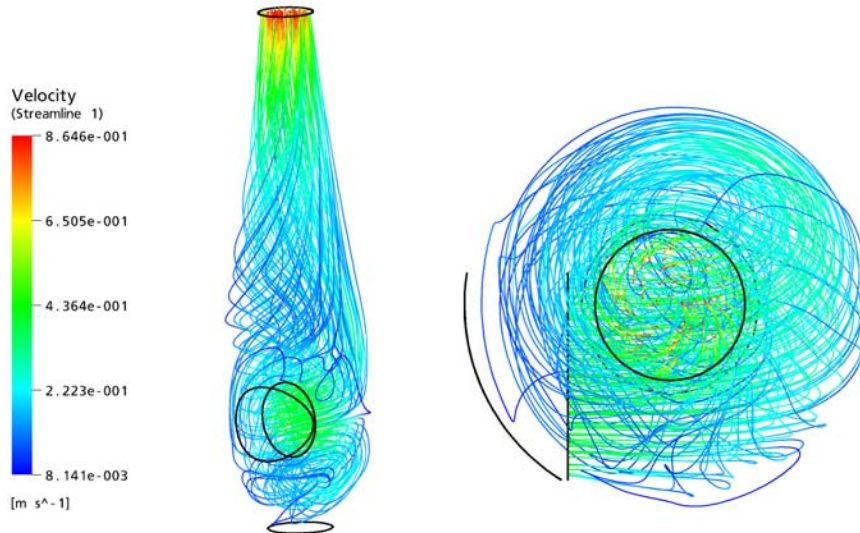


Figure 5 – Streamline within Growth Section (Left: Isometric View , Right: Top View)

The resultant levels of super-saturation within the interior volume are shown in Figure 6. As can be seen by viewing super-saturation profiles on cross-sectional planes perpendicular to the main axis of the condenser, the spatial homogeneity of the super-saturation increases continuously as the flow approaches the outlet, with a near-center super-saturation value of 1.375 and global maximum value of 1.521 near the inlet. A small recirculation zone is evident to the left of the inlet plume, caused primarily by the induced cyclonic rotation within the volume. However, this recirculation is damped by viscous dissipation as the flow continues upwards towards the outlet.

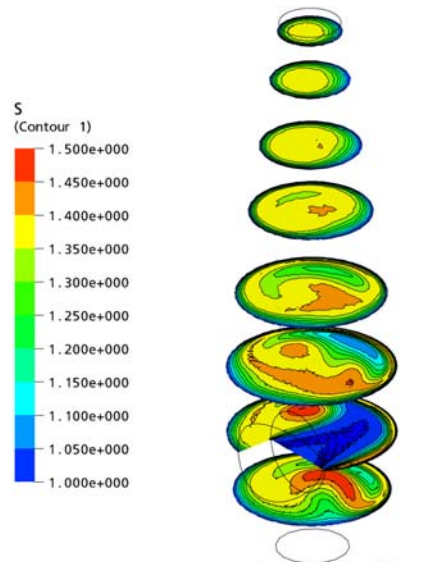


Figure 6 – Super-saturation Profiles

Using profiles of the super-saturation and temperature, a profile of the Kelvin-equivalent diameter can be calculated by:

$$D_k = \frac{4\sigma_s M_w}{\rho_l R_g T \ln(S)} \quad \text{Equation 3}$$

where σ_s , M_w , and ρ_l are the surface tension, molecular weight and density of the condensing liquid, respectively, and R_g is the universal gas constant.

As shown in Figure 7, the cross-sectional contour plots of Kelvin-equivalent diameter again show a reduction in variation as the flow approaches the exit. The exit centerline Kelvin diameter is 8.7nm with a global model minimum of 6.8nm.

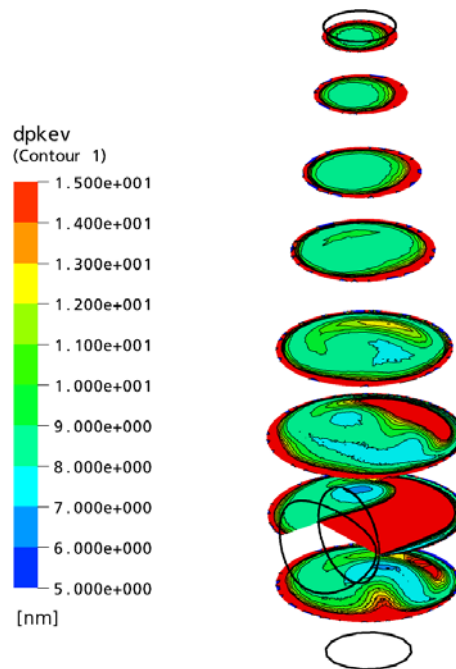


Figure 7- Kelvin Equivalent Diameter Profiles

Some variation of the Kelvin-equivalent diameter is present, and it is important to quantify the impact of this variation on the CPC performance. One technique to determine the effect of the variation on expected particle nucleation and growth is to introduce theoretical particles into the model and track their activation and growth. Using the particle tracking module within the CFD code, particles with known diameters are introduced into the volume, and the level of super-saturation that they experienced was tracked. When a particle reached a level of super-saturation such that the Kelvin-equivalent diameter was equal to or less than the diameter of the particle, it is assumed to have nucleated and grown to an optically detectable size. Tracking these values and introducing a range of particles from 5nm to 20nm facilitated prediction of the activation curve for this growth technique (Figure 8).

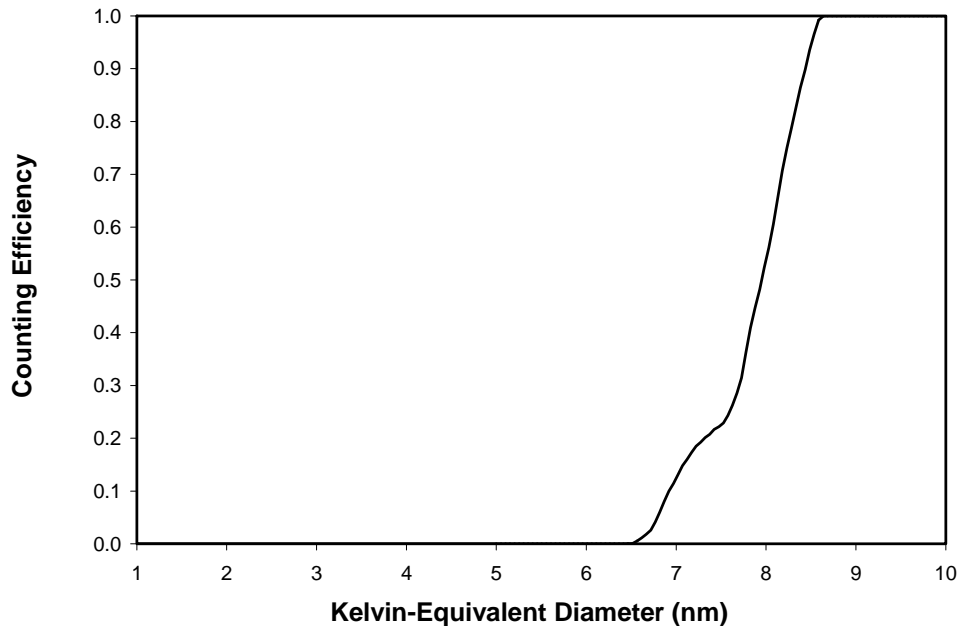


Figure 8 – Theoretical Counting Efficiency Curve for SFM Method

The resulting counting efficiency curve (Figure 8) shows a surprisingly steep slope with a range of only 1.6nm for a activation efficiency from 5% to 95%, and a predicted 50% cut point of 8.3nm. The small predicted hump from approximately 6.5 to 7.5 nm is the result of a small pocket of high super-saturation located within the bottom of the mixing geometry. This small volume below the inlet is necessary because it acts as a collection area for condensed liquid and contributes only slightly to the expected counting efficiency curve because of the small flow rate through that region.

EXPERIMENTAL VERIFICATION

To determine the actual counting efficiency for the system, the apparatus shown in Figure 9 was used to generate a monodisperse test aerosol. An evaporation-condensation system (Scheibel and Porstendörfer, 1983) was used to generate test aerosols of NaCl and Ag. Using a dilution bridge to control the concentration, the aerosol was transported to a differential mobility analyzer (DMA) for size classification. The DMA operated at a 10:1 ratio of sheath to aerosol flow rate controlled by a MSP Model 1500 Aerosol Generation and Measurement system. The size-classified aerosol was mixed with a particle-free make-up flow to provide the necessary volumetric flow rate for the MSP Model 1120 WCPC and a faraday-cup electrometer (FCE), which served as the concentration reference. The MSP Model 1120, which features the SFM growth section, was operated at a volumetric flow rate of 1.0 L/min. The FCE was operated at 2.0 L/min to ensure at least 10fA of current at a concentration of 1800 particles per cm³.

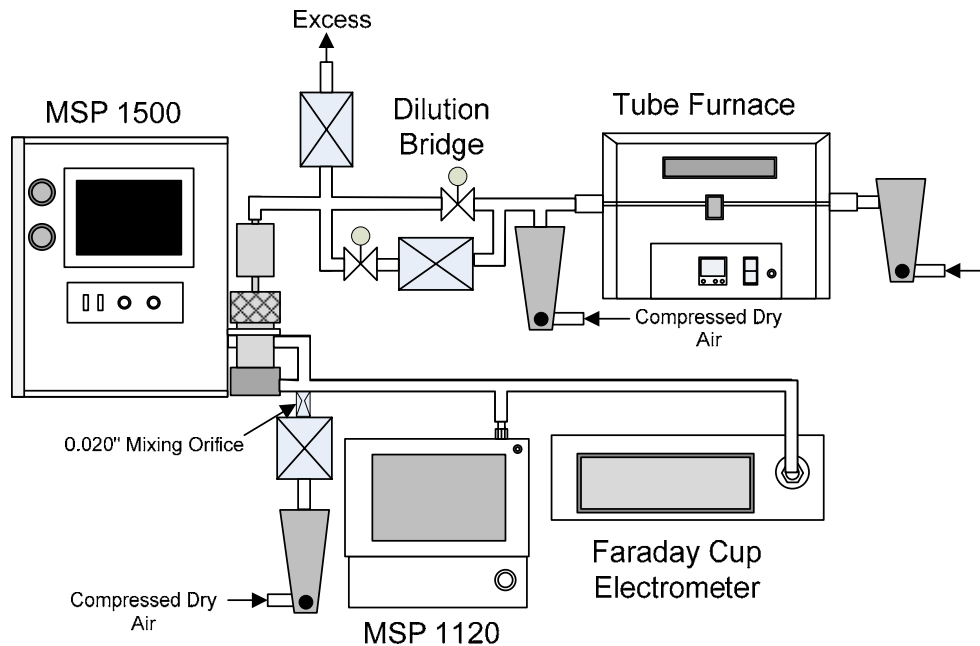


Figure 9 – Experimental setup for measurement of CPC counting efficiency curve.

For each particle size tested, the MSP 1120 and Faraday Cup Electrometer sampled continuously for 60 sec, yielding the total number count and average current, respectively. The concentration for the 60-sec interval was then computed. The classified NaCl particle diameters ranged from 3.5nm to 100nm, while for the Ag test aerosol, the upper diameter was limited to 30nm because of the maximum temperature rating of the tube furnace.

The results for the Ag aerosol show the expected trend of diminishing counting efficiency with decreasing particle size (Figure 10). Using a three-parameter exponential fit (Equation 4) and minimization of the least square error, the resulting 50% counting efficiency is determined to be 8.2nm. This value is very near the predicted 50% counting efficiency of 8.3nm predicated by the CFD model, a result that is most likely coincidental. Additional measurements would be necessary to determine if this model is valid for a variety of inlet and wall temperatures before such agreement can be accepted at face value.

$$\eta = 1 - D_3 e^{(D_1 - D_p) / D_2} \quad \text{Equation 4}$$

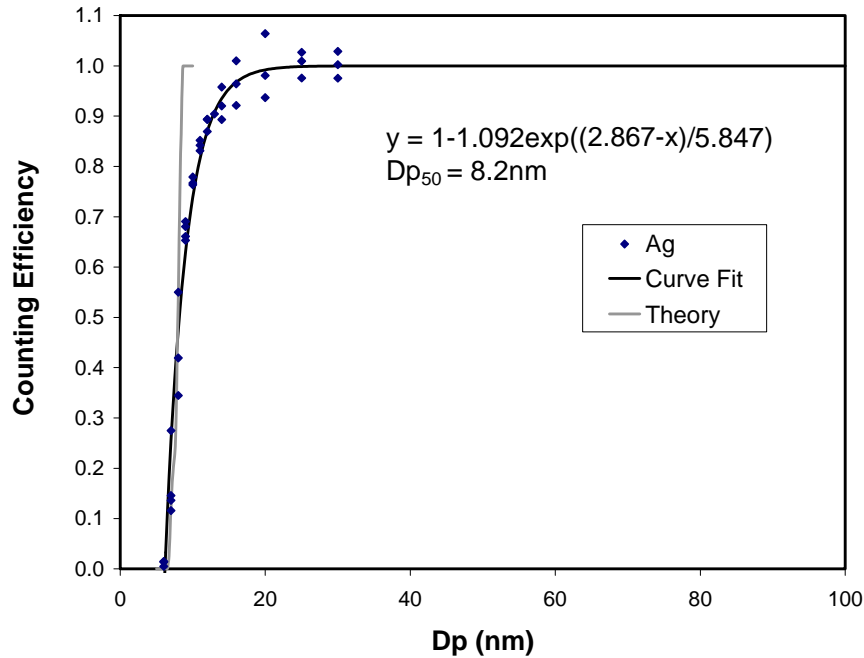


Figure 10 – Counting efficiency curve with Ag aerosol

As shown in Figure 10, the resulting three-parameter fit for the NaCl data shows a 50% counting efficiency at 3.9nm, well below the predicted cut point of 8.3nm, and the measured 8.2nm cut point of Ag. This large difference is expected and is caused by two primary effects. The first effect is the deliquescence of the NaCl test aerosol in the warm, wet saturator, resulting in the growth of particles before their entry into the growth section. Biskos et. al.(2006) found this effect to be significant for small particles, with 10nm particles increasing by a factor of 1.7 in diameter when exposed to high humidity environments. The second effect, which explains the large deviation from the predicated theory, is the assumption in the activation model that the particles are comprised of pure working fluid. Since the test aerosol now consists of a NaCl-water mixture, due to water uptake during deliquescence in the saturator, the resulting surface vapor pressure is less than that of pure water and, thereby depressing the Kelvin-equivalent diameter. This effect was also observed by Hering and Stolzenburg (2005) in which the effective cut point of the TSI 3785 varied significantly with the water solubility of the aerosol material.

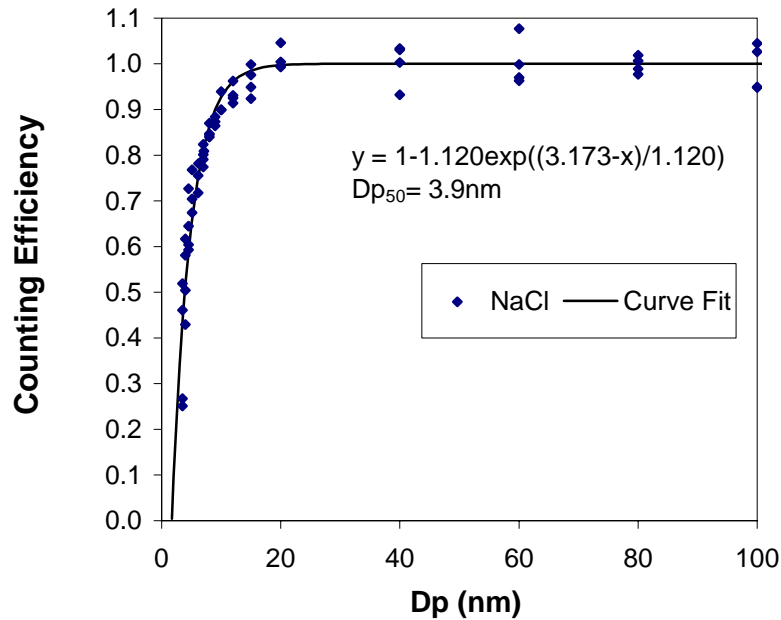


Figure 11- Counting efficiency curve with NaCl aerosol

CONCLUSION

A new, water-based condensation particle counter, based on the single-flow mixing approach (SFM) has been developed and proven experimentally. A CFD model of the internal flow, temperature and vapor profiles was generated for this method. Using the results from the CFD model, a theoretical study of the counting efficiency was performed, with a predicted 50% counting efficiency at 8.3nm for non-hygroscopic particles for the SFM method.

An empirical verification of the modeled counting efficiency of the SFM growth technique was performed using MSP's Model 1120 CPC. The measured 50% counting efficiency diameter was 8.2nm for Ag aerosol and 3.9nm for NaCl aerosol. The reduction in the 50% counting efficiency diameter is the result of a compound effect: water uptake by NaCl particles, which increases their size before entering into the growth section, and subsequent reduction of the equilibrium vapor pressure of water over the resulting NaCl-water particles, resulting in a decrease of the Kelvin diameter.



REFERENCES

- Agarwal, J.K., and Sem, G.J. (1980) Continuous Flow, Single-Particle-Counting Condensation Nucleus Counter, *J. Aerosol Sci.* 11:343-37
- Biskos, G.Maliowski, L., Russel, L.M., Buseck, P.R., and Martin, S.T. (2006) Nanosize Effect on the Deliquescence and the Efflorescence of Sodium Chloride Particles. *Aerosol Sci. Technol.*,40:97-106
- Bolz, R.E. and Tuve, G.L. (1976) *Handbook of Tables for Applied Engineering Science*. 2nd Edition, CRC Press, New York.
- Brucard, J., Delattre, P., Madelaine, G., and Pourprix, M. (1976) Detection of Ultra-Fine Particles by Means of a Continuous Flux Condensation Nuclei Counter. *In Fine Particles: Aerosol Generation, Measurement, Sampling, and Analysis*, edited by B.Y.H. Liu. New York, Academic Press, New York, pp. 565-580.
- Hering, S. Stolzenburg, M., Quant, F., Oberreit, D., and Keady, P. (2005) A Laminar Flow, Water-Based Condensation Particle Counter(WCPC), *Aerosol Sci. Technol.*, 39: 659-672.
- Liu, B. Y. H., Dinh, T. M., Dick, W. D., Collins A., and Romay, F. (2011) Method and Apparatus for Counting Particles in a Gas. *U.S. Patent Application Publication*, Pub. No. US2011/0091649A1.